Electronic Supplementary Material (ESI): Supporting Information

rGO functionalized (Ni, Fe)-OH for an efficient trifunctional catalyst in low-cost hydrogen generation via urea decomposition as a proxy anodic reaction

Nabeen K. Shrestha,[a] Supriya A. Patil,*[b] Akbar I. Inamdar,[a] Sunjung Park,[a] Seungun Yeon,[a] Giho Shin,[a] Sangeun Cho,[a] Hyungsang Kim,[a] Hyunsik Im[a*]

[a]Division of Physics and Semiconductor Science, Dongguk University-Seoul, Seoul 04620, Republic of Korea.

[b]Department of Nanotechnology and Advanced Materials Engineering, Sejong University, Seoul-05006, Republic of Korea.

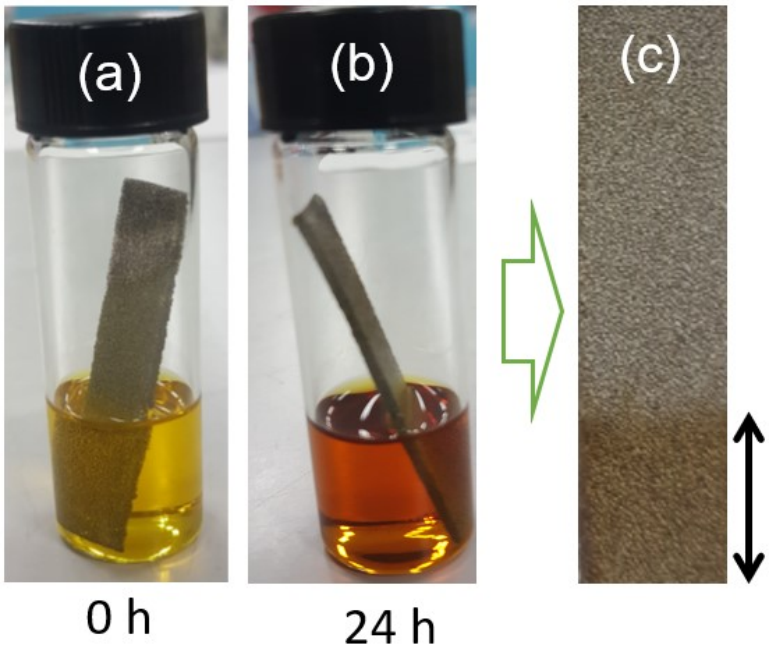

Figure S1. Photo images of (a) nickel foam immersed in an ethylene glycol-water (80:20 vol%) mixture solution containing 20 μmole mL^{-1} of $FeCl_3.6H_2O$ and 1 mgL^{-1} rGO at 25°C. Arrow shows the deposited film.

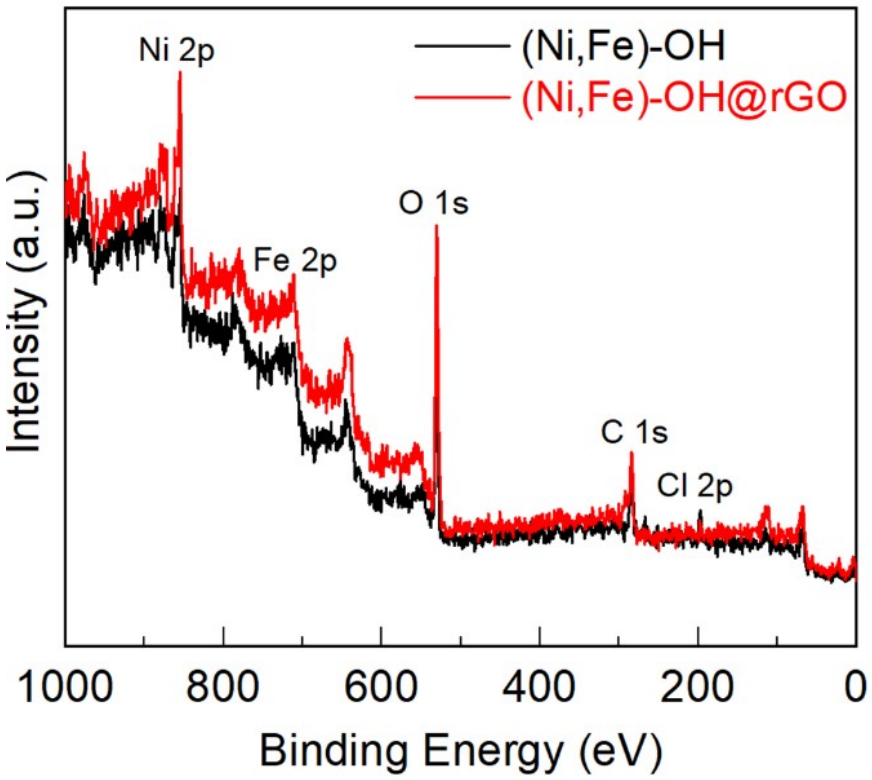

Figure S2. XPS survey spectra of the (Ni,Fe)-OH/NF and (Ni,Fe)-OH@rGO/NF electrodes.

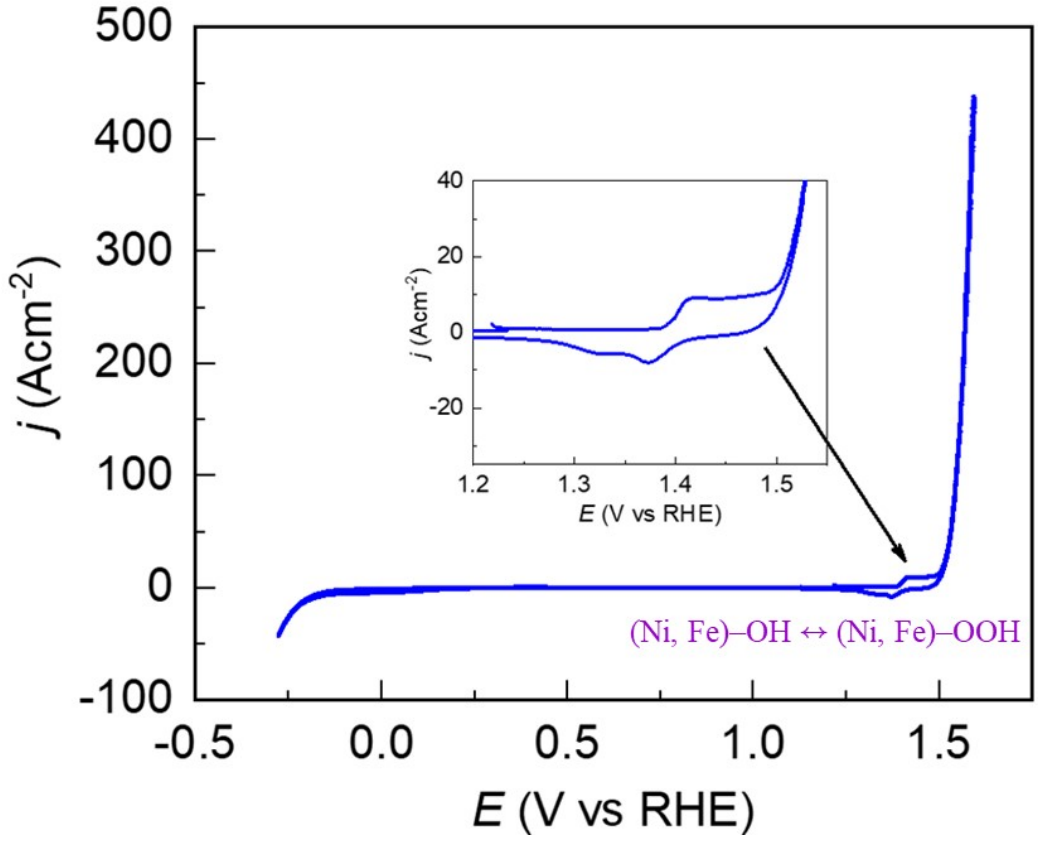

Figure S3. Cyclic voltammogram (CV) of the (Ni,Fe)-OH/NF electrode in the 1.0 M KOH electrolyte at a scan speed of 5 mVs^{-1}. The inset image shows the enlarged CV view around the redox peak.

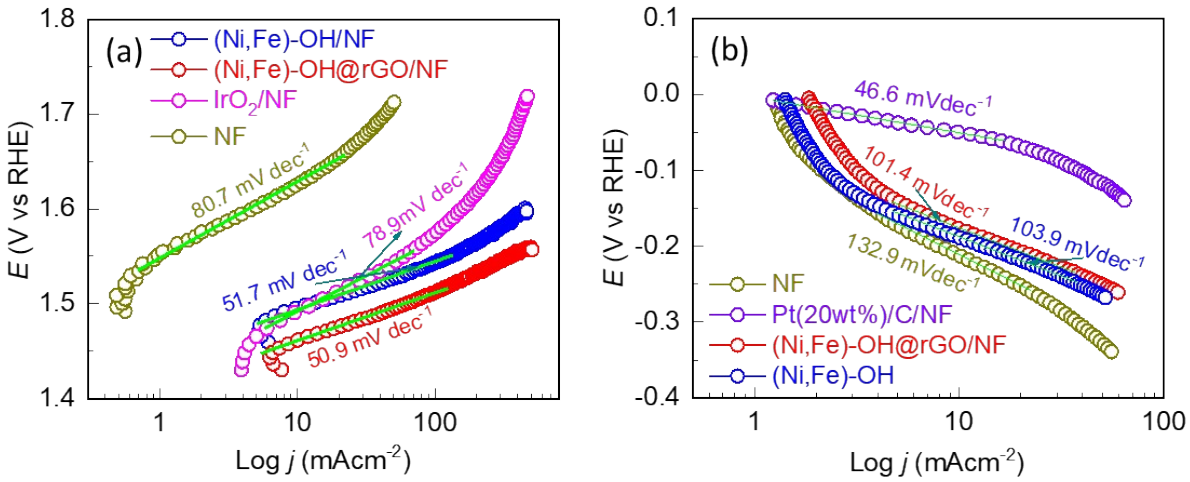

Figure S4. Tafel slopes extracted from the corresponding LSV polarization curves for (a) OER and (b) HER.

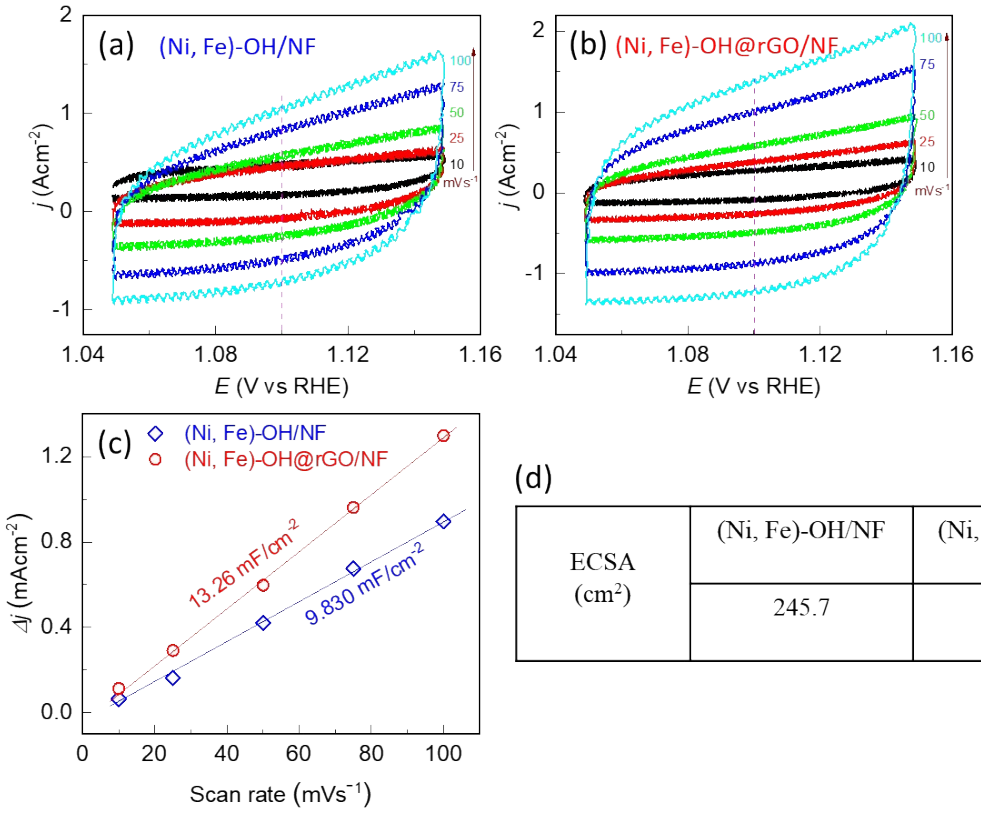

(d)

ECSA (cm^2)	(Ni, Fe)-OH/NF	(Ni, Fe)-OH@rGO/NF
	245.7	331.5

Figure S5. Cyclic voltammograms exhibited by the (a) (Ni,Fe)-OH/NF and (b) (Ni,Fe)-OH@rGO/NF electrodes at various scan rates in 1.0 M KOH solution. Δj vs scan rate linear plots providing the double layer capacitance (C_{dl}) of the electrodes by the slope of the plots. (d) ECSA of the electrodes determined by the relation C_{dl}/C_s, where C_s is the specific capacitance of the electrodes in 1.M KOH solution and is generally taken as 0.04 $mFcm^{-2}$.

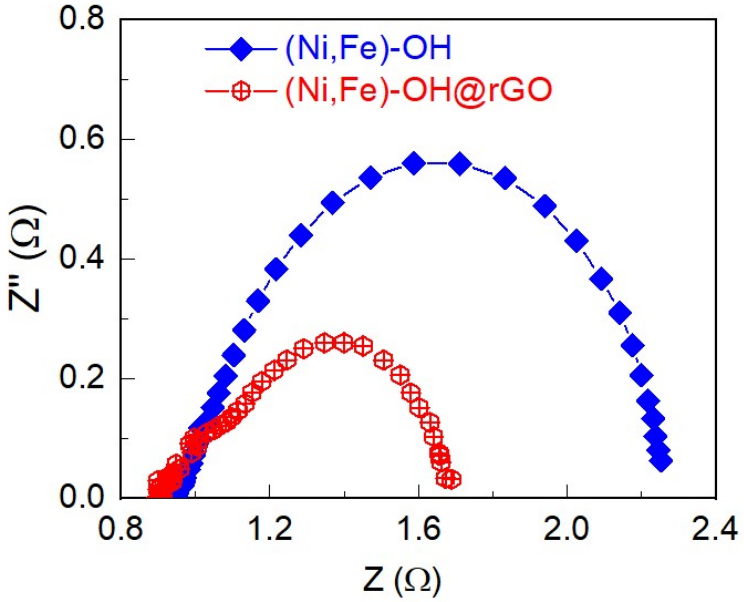

Figure S6. Nyquist spectra measured at 1.48 V (vs. RHE) in 1.0 M KOH solution.

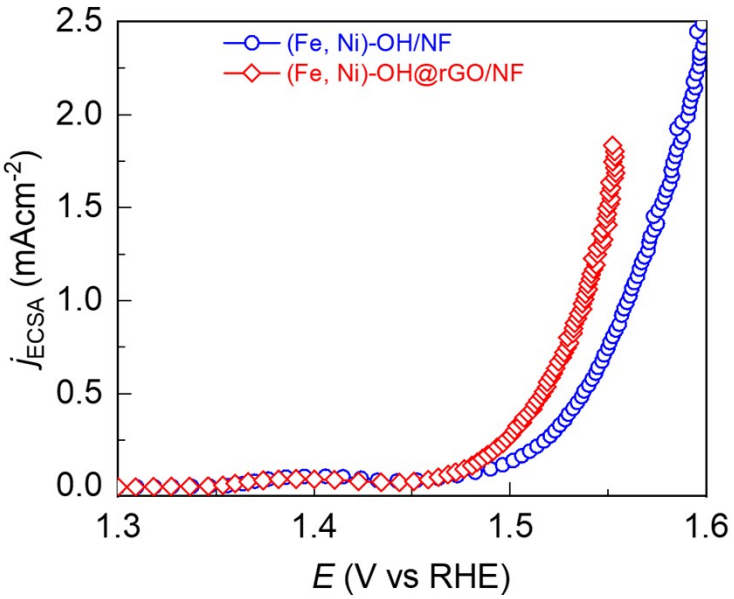

Figure S7. ESCA specific LSV polarization curves of the (Ni,Fe)-OH/NF and (Ni,Fe)-OH@rGO/NF electrodes in 1.0 M KOH solution.

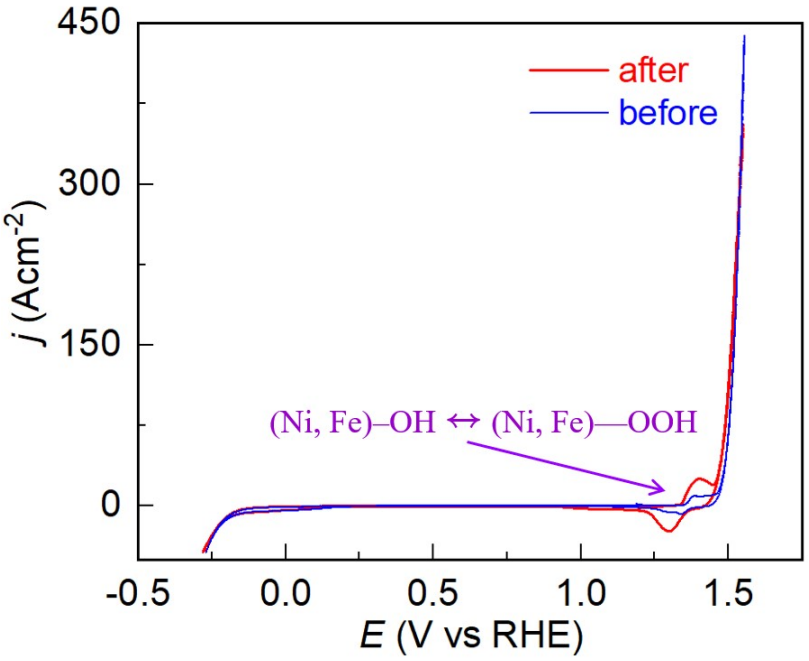

Figure S8. Cyclic voltammogram (CV) of the (Ni,Fe)-OH@rGO/NF electrode before and after the long-term stability test for 48 h (24 h at 250 $mAcm^{-2}$ and 24 h at 500 $mAcm^{-2}$). A scan speed of 5 mVs^{-1} was employed.

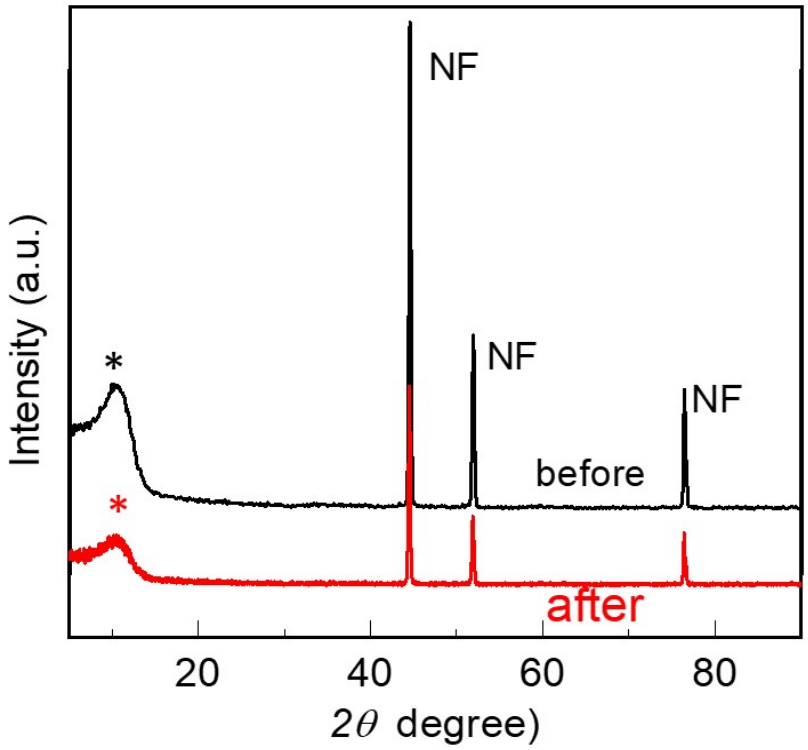

Figure S9. XRD patterns of the (Ni,Fe)-OH@rGO/NF electrode before and after the long-term stability test for 48 h (24 h at 250 $mAcm^{-2}$ and 24 h at 500 $mAcm^{-2}$). The broad (*) peak is from the film, while other peaks are from the nickel foam (NF) substrate.

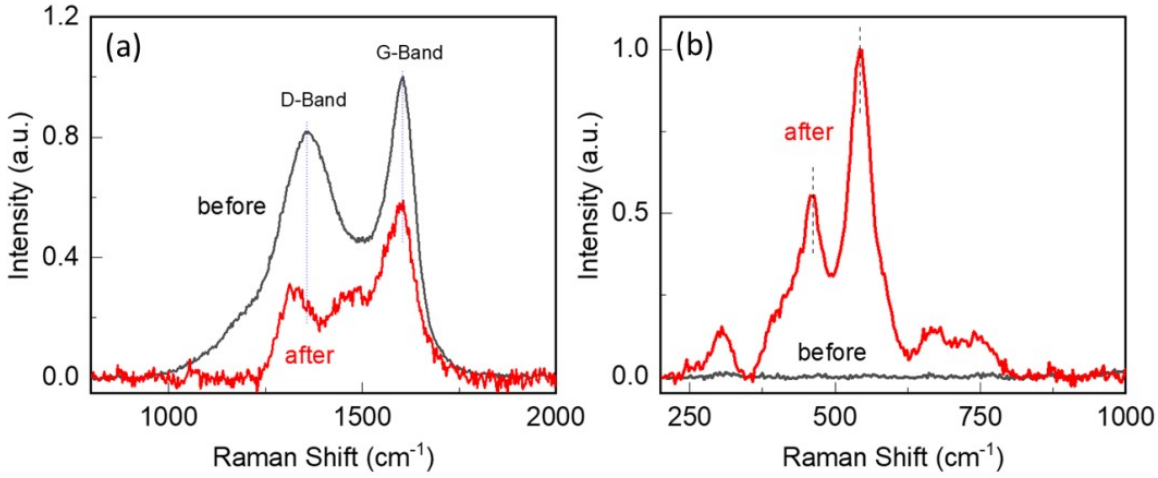

Figure S10. Raman spectra of the (Ni,Fe)-OH@rGO/NF electrode before and after the long-term stability test for 48 h (24 h at 250 $mAcm^{-2}$ and 24 h at 500 $mAcm^{-2}$).

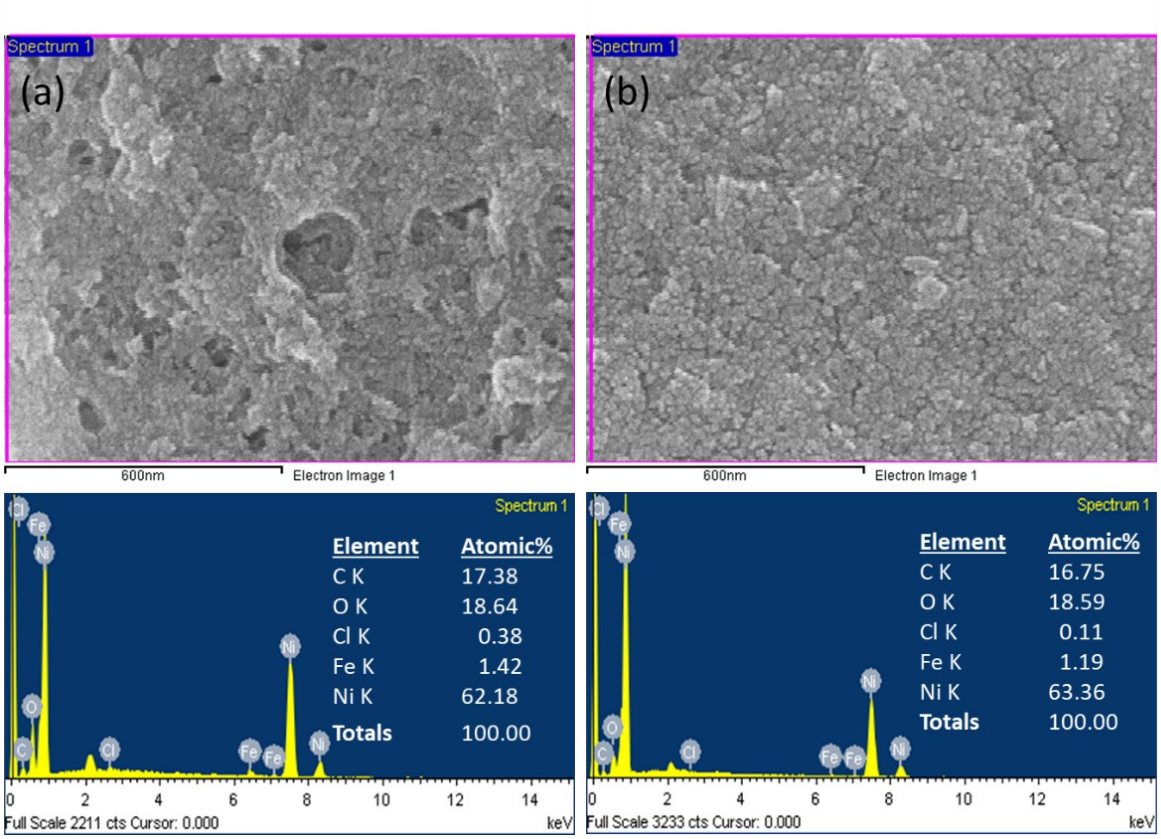

Figure S11. SEM images of the (Ni,Fe)-OH@rGO/NF electrode (a) before and (b) after the long-term stability test for 48 h (24 h at 250 $mAcm^{-2}$ and 24 h at 500 $mAcm^{-2}$). (c) and (d) show the EDS elemental spectra and atomic percentages of the main constituting elements.

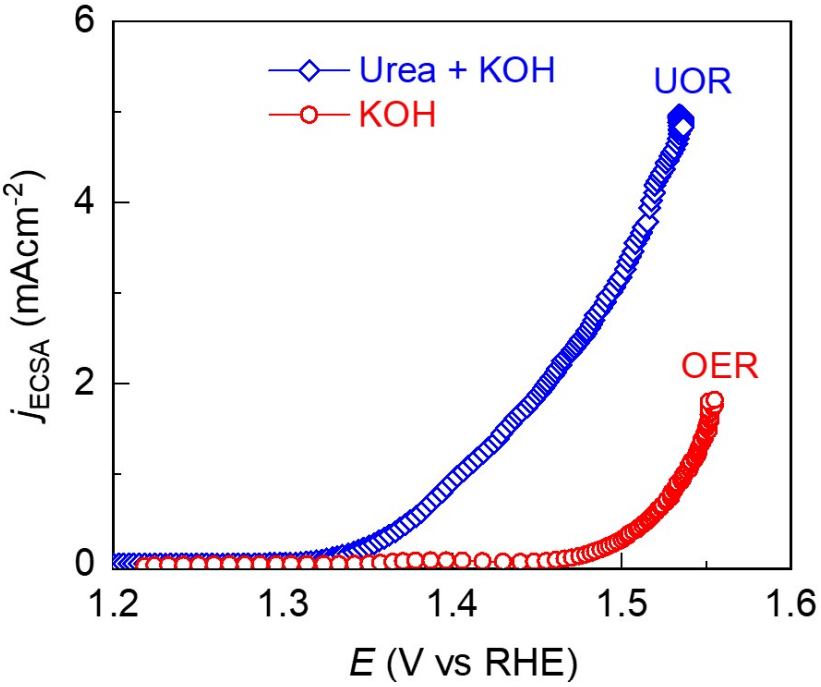

Figure S12. ECSA specific LSV polarization curves of the (Ni,Fe)-OH@rGO/NF electrode in 1.0 M KOH and 0.33 M urea-supplemented 1.0 M KOH aqueous electrolytes.

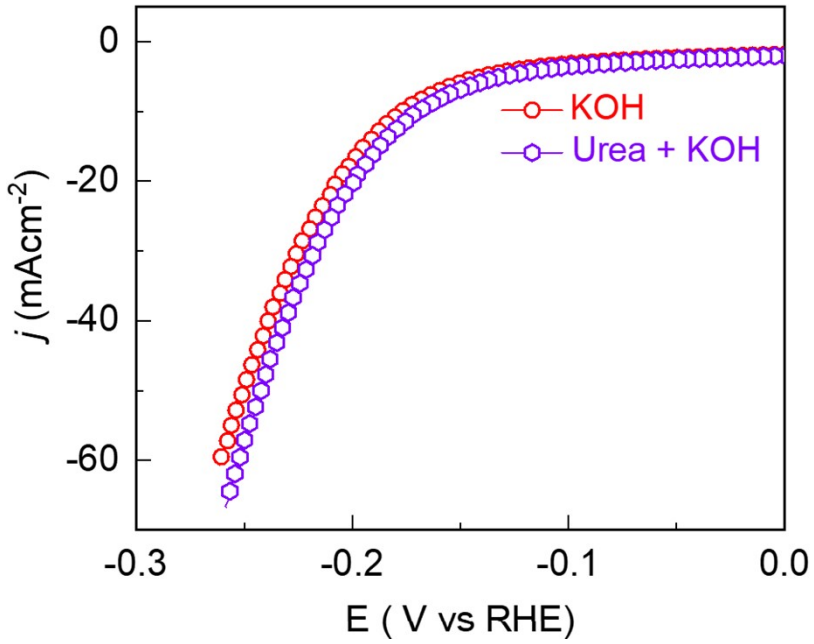

Figure S13. Cathodic polarization curves of the (Ni,Fe)-OH@rGO/NF electrode in 1.0 M KOH and 0.33 M urea-supplemented 1.0 M KOH electrolytes, revealing that the replacement of OER by UOR does not influence the HER activity of the electrode.

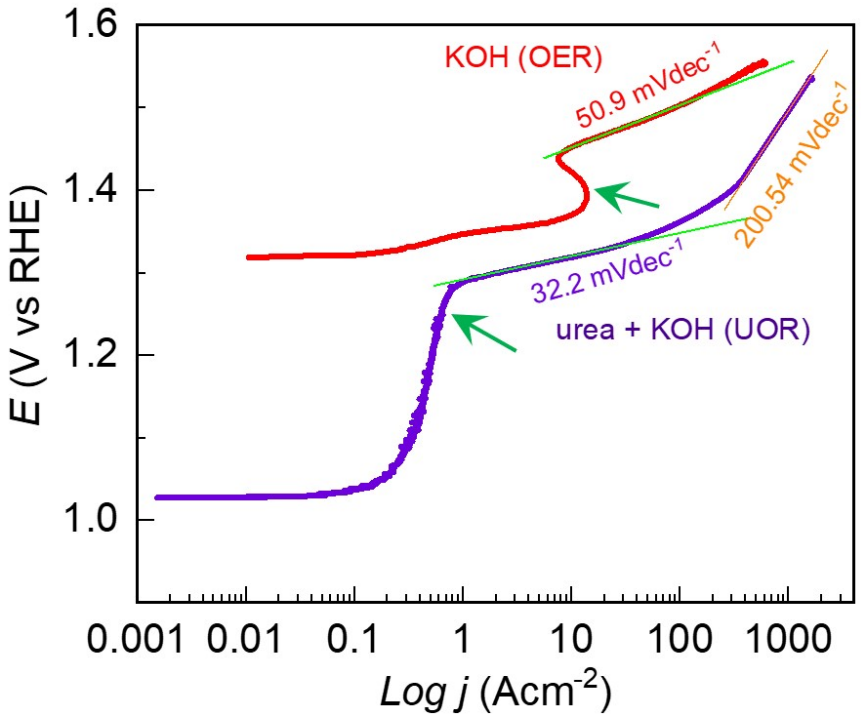

Figure S14. Tafel plots for UOR and OER plotted in the full potential ranges of the corresponding LSV polarization curves shown in 'Figure 9a'.

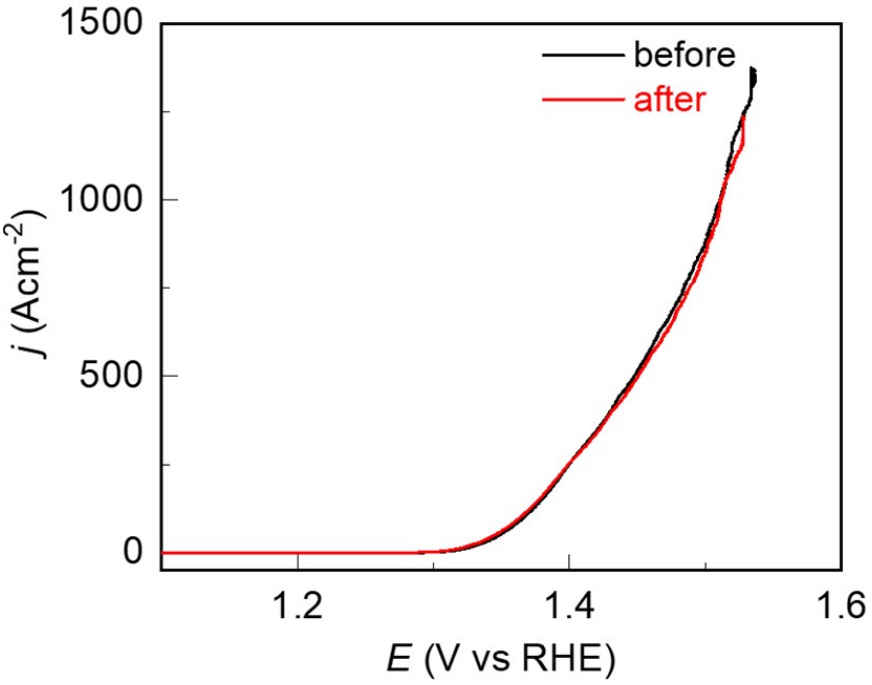

Figure S15. Anodic polarization curves of the (Ni,Fe)-OH@rGO/NF electrode in the 0.33 M urea-supplemented 1.0 M KOH electrolyte before and after the long-term stability test for 24 h at 10 $mAcm^{-2}$.

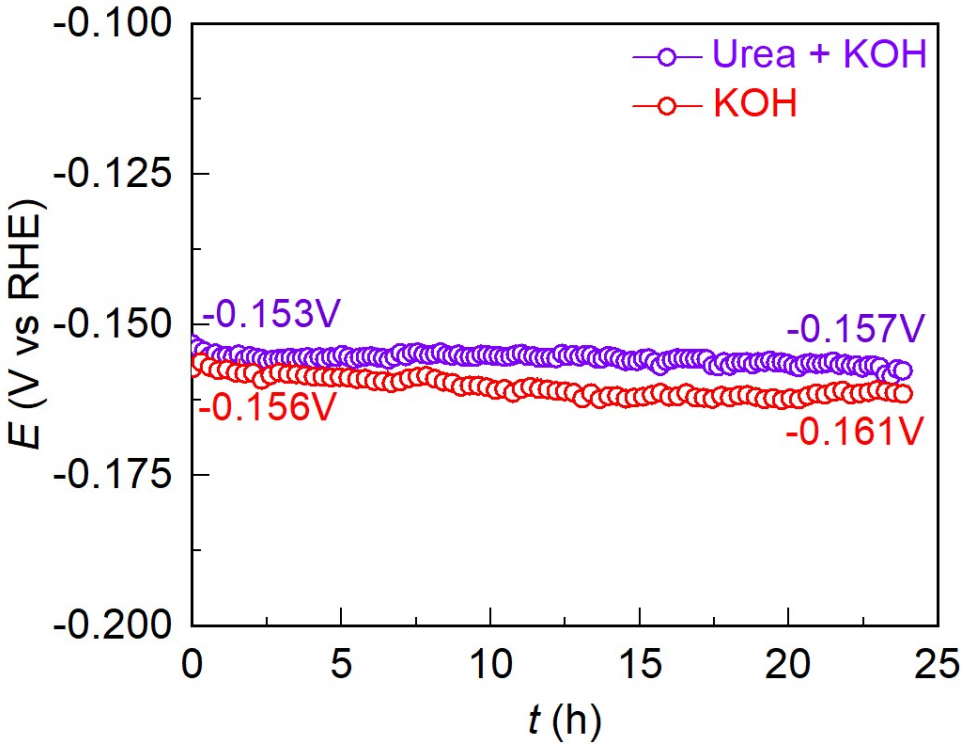

Figure S16. Chronopotentiometric stability test showing the long-term electrochemical durability of the (Ni,Fe)-OH@rGO/NF electrode against the HER in urea-free and 0.33 M urea-supplemented 1.0 M KOH electrolytes at -10 $mAcm^{-2}$.

Table S1. Comparison of OER performance for (Ni,Fe)-OH@rGO/NF and (Ni,Fe)-OH/NF with those of state-of-the art electrocatalysts under alkaline conditions.

	Electrode materials	Electrolyte	*j* ($mAcm^{-2}$)	Overpotential (mV)	Tafel slope ($mVdec^{-1}$)	Ref
1	(Ni,Fe)-OH@rGO/NF	1 M KOH	10 50 100 250 500	230 250 270 300 320	50.9	**This work**
	(Ni,Fe)-OH/NF		10 50 100 250	260 290 310 340	71.7	
	IrO_2/NF		10 50 100 250	260 310 340 400	78.9	
3	NFN-MOF/NF		10 250	240 335	58.8	1
4	NiFe/$NiCo_2O_4$/NF		10	240	38.8	2
5	MFN-MOFs(2:1)/NF		50	235	55.4	3
6	Ni-QDs@NC@rGO		10	265	65.0	4
7	Fe-O-$Ni(OH)_2$/NF		10 100	185 220		5
8	NiFeOx/NF		100	260	28.0	6
9	Ni-Fe NP/CFP		10 20 100	210 230 270	-	7
10	NiFe-LDH/Mxene/NF		10	229	44.0	8
11	Hier-NiFe@sCNTs		30 100	210 271	65.7	9

Table S2. Comparison of UOR performance for (Ni,Fe)-OH@rGO/NF with those of reported high-performance electrocatalysts.

	Electrode materials	Electrolyte	*j* ($mAcm^{-2}$)	Cell potential (V) vs RHE	Overpotential (V)	Ref.
1	(Ni,Fe)-OH@rGO/NF	1 M KOH + 0.33 urea	100 500 1000 1600	1.35 1.43 1.49 1.53	0.98 1.06 1.12 1.16	**This work**
	NC-PB@CNT	1 M KOH + 0.33 urea	100	1.41	1.04	10
2	NiS@Ni_2S/$NiMoO_4$	1 M KOH + 0.5 urea	100 450	1.46 1.78	1.09 1.41	11
	NiIr-MOF/NF	1 M KOH + 0.5 urea	100 300	1.349 1.350	0.979 0.980	12
3	NiFeRh-LDH	1 M KOH + 0.33 urea	100 500	1.37 1.44	1.00 1.07	13
	NFHC	1 M KOH + 0.5 urea	100	1.40	1.03	14
4	NiMoO-Ar/NF	1 M KOH + 0.5 urea	100 300	1.42 1.52	1.05 1.15	15
6	V_0-rich-$CoMoO_4$/NF	1 M KOH + 0.5 urea	100	1.51	1.14	16
8	CoS_2-MoS_2/NF	1 M KOH + 0.5 urea	100 350	1.33 1.36	0.96 0.99	17

References

(1) Yu, H.; Quan, T.; Mei, S.; Kochovski, Z.; Huang, W.; Meng, H.; Lu, Y. Prompt Electrodeposition of Ni Nanodots on Ni Foam to Construct a High-Performance Water-Splitting Electrode: Efficient, Scalable, and Recyclable. *Nano-Micro Lett.* **2019**, *11* (1), 41.

(2) Xiao, C.; Li, Y.; Lu, X.; Zhao, C. Bifunctional Porous NiFe/NiCo2O4/Ni Foam Electrodes with Triple Hierarchy and Double Synergies for Efficient Whole Cell Water Splitting. *Adv. Funct. Mater.* **2016**, *26* (20), 3515–3523.

(3) Senthil Raja, D.; Lin, H. W.; Lu, S. Y. Synergistically Well-Mixed MOFs Grown on Nickel Foam as Highly Efficient Durable Bifunctional Electrocatalysts for Overall Water Splitting at High Current Densities. *Nano Energy* **2019**, *57*, 1–13.

(4) Chen, Z.; Xu, H.; Ha, Y.; Li, X.; Liu, M.; Wu, R. Two-Dimensional Dual Carbon-Coupled Defective Nickel Quantum Dots towards Highly Efficient Overall Water Splitting. *Appl. Catal. B Environ.* **2019**, *250*, 213–223.

(5) Zhong, D.; Zhang, L.; Li, C.; Li, D.; Wei, C.; Zhao, Q.; Li, J.; Gong, J. Nanostructured NiFe (Oxy)Hydroxide with Easily Oxidized Ni towards Efficient Oxygen Evolution Reactions. *J. Mater. Chem. A* **2018**, *6* (35), 16810–16817.

(6) Wang, J.; Ji, L.; Chen, Z. In Situ Rapid Formation of a Nickel-Iron-Based Electrocatalyst for Water Oxidation. *ACS Catal.* **2016**, *6* (10), 6987–6992.

(7) Suryanto, B. H. R.; Wang, Y.; Hocking, R. K.; Adamson, W.; Zhao, C. Overall Electrochemical Splitting of Water at the Heterogeneous Interface of Nickel and Iron Oxide. *Nat. Commun.* **2019**, *10* (1), 5599.

(8) Yu, M.; Wang, Z.; Liu, J.; Sun, F.; Yang, P.; Qiu, J. A Hierarchically Porous and Hydrophilic 3D Nickel–Iron/MXene Electrode for Accelerating Oxygen and Hydrogen Evolution at High Current Densities. *Nano Energy* **2019**, *63*, 103880.

(9) Ahn, S. H.; Manthiram, A. Single Ni Atoms and Clusters Embedded in N-Doped Carbon

"Tubes on Fibers" Matrix with Bifunctional Activity for Water Splitting at High Current Densities. *Small* **2020**, *16* (33), 2002511.

(10) Patil, S. A.; Cho, S.; Jo, Y.; Shrestha, N. K.; Kim, H.; Im, H. Bimetallic Ni-Co@hexacyano Nano-Frameworks Anchored on Carbon Nanotubes for Highly Efficient Overall Water Splitting and Urea Decontamination. *Chem. Eng. J.* **2021**, *426*, 130773.

(11) Sha, L.; Liu, T.; Ye, K.; Zhu, K.; Yan, J.; Yin, J.; Wang, G.; Cao, D. A Heterogeneous Interface on NiS@Ni3S2/$NiMoO_4$heterostructures for Efficient Urea Electrolysis. *J. Mater. Chem. A* **2020**, *8* (35), 18055–18063.

(12) Xu, Y.; Chai, X.; Ren, T.; Yu, S.; Yu, H.; Wang, Z.; Li, X.; Wang, L.; Wang, H. Ir-Doped Ni-Based Metal-Organic Framework Ultrathin Nanosheets on Ni Foam for Enhanced Urea Electro-Oxidation. *Chem. Commun.* **2020**, *56* (14), 2151–2154.

(13) Sun, H.; Zhang, W.; Li, J. G.; Li, Z.; Ao, X.; Xue, K. H.; Ostrikov, K. K.; Tang, J.; Wang, C. Rh-Engineered Ultrathin NiFe-LDH Nanosheets Enable Highly-Efficient Overall Water Splitting and Urea Electrolysis. *Appl. Catal. B Environ.* **2021**, *284* , 119740.

(14) Feng, Y.; Wang, X.; Dong, P.; Li, J.; Feng, L.; Huang, J.; Cao, L.; Feng, L.; Kajiyoshi, K.; Wang, C. Boosting the Activity of Prussian-Blue Analogue as Efficient Electrocatalyst for Water and Urea Oxidation. *Sci. Rep.* **2019**, *9* (1), 15965.

(15) Yu, Z.-Y.; Lang, C.-C.; Gao, M.-R.; Chen, Y.; Fu, Q.-Q.; Duan, Y.; Yu, S.-H. Ni–Mo–O Nanorod-Derived Composite Catalysts for Efficient Alkaline Water-to-Hydrogen Conversion via Urea Electrolysis. *Energy Environ. Sci.* **2018**, *11* (7), 1890–1897.

(16) Liu, Z.; Teng, F.; Yuan, C.; Gu, W.; Jiang, W. Defect-Engineered CoMoO4 Ultrathin Nanosheet Array and Promoted Urea Oxidation Reaction. *Appl. Catal. A Gen.* **2020**, *602* (May), 117670.

(17) Li, C.; Liu, Y.; Zhuo, Z.; Ju, H.; Li, D.; Guo, Y.; Wu, X.; Li, H.; Zhai, T. Local Charge Distribution Engineered by Schottky Heterojunctions toward Urea Electrolysis. *Adv. Energy Mater.* **2018**, *8* (27), 1801775.